Control and management Strategy of a Generation System Made By Variable-Speed Wind Turbine and Super-Capacitor Energy Storage System for Standalone Applications

Youssef KRIM, Saber KRIM, and Mohamed Faouzi MIMOUNI

[a]National Engineering School of Monastir, Electrical Engineering Department, Research Unit "Industrial Systems Study and Renewable Energy", Avenue Ibn El Jazzar 5019, University of Monastir–Tunisia

Abstract: This paper deals with the problems of intermittency of primary source of wind energy and the external disturbances. Subsequently, a power management and a robust control of a standalone energy production unit are presented. This production unit comprising a variable speed wind turbine coupled to a Permanent Magnet Synchronous Generator (PMSG) and a module of Super-Capacitors (SC) that is considered as an Energy Storage System (ESS). This unit feeds a three-phase load by means of an inverter and an RLC filter. In order to assure a control strategy which has a very good performance despite the high nonlinearity of wind systems and an intermittence form of wind power, a second-order sliding mode control based on a super-twisting algorithm is applied to a PMSG. Then, a power management strategy is applied to the SC using a buck-boost converter according to load instructions and wind speed fluctuations. The response of the power algorithm enables to ensure the power flow exchange between the production unit and the power consumers and to protect the ESS against overcharge and excess discharge to ensure safe operation. Finally, using PI controllers, the inverter adjusts the capacitors voltages and currents at the output of the RLC filter with the nominal frequency and voltage. The simulation results show the robustness of the implanted control strategy.

Keywords: Wind turbine, Supercapacitors, Second-order sliding mode control, Super-twisting algorithm, Voltage source inverter, Power management algorithm.

1. Introduction

Faced with the depletion of fossil fuels and global warming, as well as the global growth in energy demand, the development of clean energy sources seems increasingly necessary. To meet these challenges we have to go through a transition period in which we use renewable energy [1]. The electricity from renewable sources, particularly wind and sun, is considered an interesting alternative production in electrical power systems in the world today [2]. However, their use is limited by the variability in resources that may reduce their reliability [3]. The load fluctuations according to the annual or daily periods are not necessarily correlated with the available energy resources. To overcome this limit, the preferred option for isolated sites, is certainly the use and combination of several sources with storage systems [4, 5]. The most suitable storage system is the battery, because it is a proven technology and has a good ratio performance/cost and is suitable for constant power utilization, but there is a need for regular maintenance. However, Super-Capacitors (SC) are characterized by their high efficiency energy transfer in short duration, and high reactivity and longevity [6]. It is in this context that the problematic of this paper is located: designing and optimizing a distribution generator to meet the needs of variable-load electricity.

This study focuses on wind energy conversion systems. The rapid and unexpected fluctuation of the wind is the major drawback associated with wind energy [7]. Indeed, wind generators installed worldwide are generally seen as passive energy sources [8]. For this, we will integrate an SC module as a fast storage system with a high specific power to smooth the output fluctuations of a wind turbine. The association of the wind turbine and the SC module forms our

Received: February 23rd, 2017. Accepted: September 28th, 2017
DOI: 10.15676/ijeei.2017.9.3.11

decentralized generator, which aims to ensure a continuous supply of load without fluctuations and correlate production to consumption.

In order to improve the quality of electric power produced by wind generators, a robust control insensitive to external perturbation is needed to control the wind generators [9]. A conventional vector control strategy based on proportional integral controllers will limit performances; this limitation is due to the nonlinearity of the studied system [10]. To address this problem, a nonlinear control strategy is implemented, such as neural network and fuzzy logic [11, 12]. In [13] a nonlinear control strategy based on a first-order sliding mode control was applied. This strategy had a good performance except that the chattering phenomenon was the major drawback of the practical implementation of this strategy.

In this context, the first part of this study is devoted to the modeling of different devices of the production system. This system comprises a wind turbine coupled to a Permanent Magnet Synchronous Generator (PMSG). The latter is connected via a three-phase rectifier and a common DC bus voltage with an SC module as an energy storage system. The SC allows regulating the continuous bus voltage by controlling the difference between the produced power and the required one. The produced power feeds a three-phase load by means of an inverter and an RLC filter.

In the second part, the power management supervisor and the robust control applied to our studied system are presented. Within this framework, this study is interested in a second-order sliding mode control based on a super-twisting algorithm applied to the PMSG to have a Maximum Power Point Tracking (MPPT). To control the DC bus voltage, an SC module is inserted to ensure a balance between the produced and required powers in any condition. This SC will store energy if there is an excess and will have an additional energy reserve in case of a shortage. Therefore, a power management algorithm is implemented. Finally, a Voltage Source Inverter (VSI) control is presented. The VSI control consists of two loops: a loop of adjusting the capacitors voltages with a nominal voltage and a loop of controlling the output currents of the VSI.

All of the models are represented using Matlab/Simulink software. The obtained simulation results show the effectiveness of the SC in the DC bus regulation and the good performance of the super-twisting algorithm in terms of response time.

2. Description and modelling of distribution generator

A. Description

The studied system in this paper is presented in Figureure 1. It is composed of three large parts. The first one is a wind energy conversion chain made by a wind turbine with three blades, a PMSG and a three-phase rectifier (converter 1 AC/DC). The second one is SC chain consisting of an SC module, an inductive filter and a reversible chopper (converter 2 DC/DC) used to manage internal power exchanges and to adapt the output voltages of the SC to that of the DC bus. The third part is the load, subject to variations in the power demand. The wind and SC chains form a decentralized generator connected to variable load. This connection is made through a common DC bus, a three-phase inverter (converter 3 DC/AC) that transfers power produced by the generator towards the load to ensure continuous alimentation, and an RLC filter that minimizes the harmonics generated by this inverter.

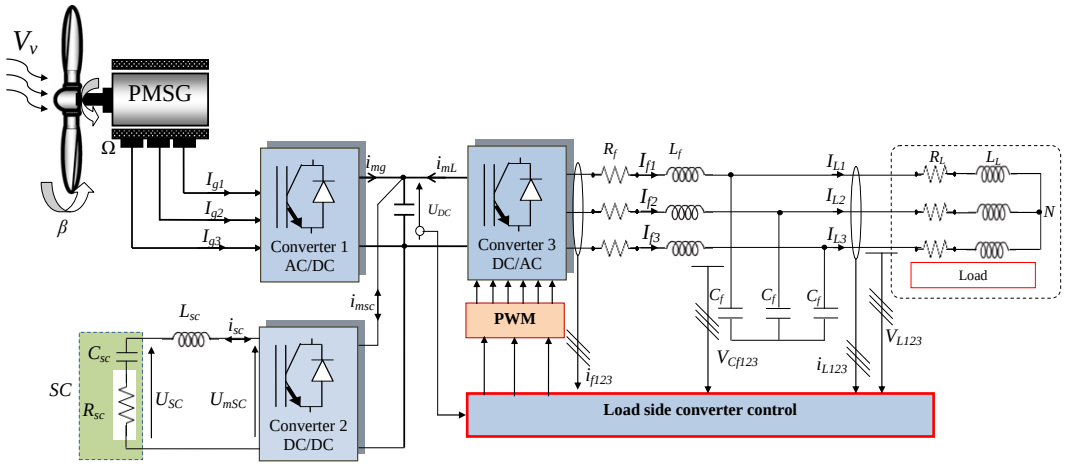

Figure 1. Structure of distributed generator

B. Wind generator modeling

The aerodynamic power P_{aer} that can be extracted from the wind and the aerodynamic torque T_{aer} are determined by the following expressions [14]:

$$P_{aer} = \frac{1}{2}\rho\pi R^2 v^3 C_p(\lambda,\beta) \tag{1}$$

$$T_{aer} = \frac{P_w}{\Omega_m} = \frac{1}{2}\rho\pi R^3 v^2 C_p(\lambda,\beta)/\lambda \tag{2}$$

where ρ is the density of air [kg/m^3], v is the wind speed [m/s], and $C_p(\lambda, \beta)$ is the power coefficient given by (3) corresponding to the aerodynamic performance of the turbine [15]. This quantity depends on the pitch angle β and the specific speed λ.

$$C_p(\lambda,\beta) = 0.5179\left(98\delta - 0.4\beta + 5\right)e^{-21\delta} + 0.068\lambda \tag{3}$$

$$\delta = \frac{1}{\dfrac{1}{\lambda + 0.089} - \dfrac{0.035}{\beta^3 + 1}};\ \lambda = \frac{R\Omega_m}{v} \tag{4}$$

with Ω_m being the mechanical speed determined by the following fundamental dynamics relation:

$$J\frac{d\Omega_m}{dt} = T_{aer} - T_{em} - f\Omega_m \tag{5}$$

where f and J are respectively the coefficient of friction and the inertia, and T_{em} is the electromagnetic torque.

An approximate example of the variation of the power coefficient $C_p(\lambda, \beta)$ according to the speed ratio λ for different β blade pitch angles is shown in Figureure 2. An increase of in pitch angle leads to a decrease in the C_p coefficient. For a given orientation of the blades, the β and λ characteristics reach a maximum for a particular value of the speed ratio. The power coefficient of the wind reflects the proportion of energy from the wind captured by the turbine. Theoretically, it is limited to 0.59, which means that it is possible to extract a maximum of 59% of the kinetic energy in the wind. In practice, it does not exceed 0.49 for the best wind turbine [16].

In this study, the curve of C_p versus λ with β=0 demonstrates an optimum value of the speed ratio (λ_{opt}=8.15) corresponding to a maximum value of the power coefficient (C_{pmax}=0.4794). The adjustment of λ to its optimal value with a power coefficient reaching C_{pmax} ensures the maximum power extraction. Equation (6) gives the expression of the maximum power obtained by using the MPPT strategy [17]:

$$\begin{cases} P_{MPPT} = T_{em-MPPT}\Omega_m \\ T_{em-MPPT} = \dfrac{1}{2}\dfrac{\rho\pi R^5 C_{p-\max}}{\lambda_{opt}^{\ 3}}\Omega_m^{\ 2} \end{cases} \tag{6}$$

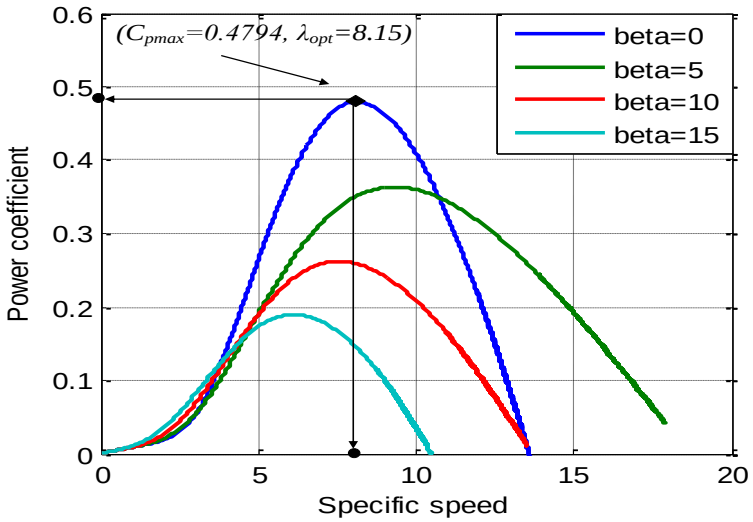

Figure 2. *Characteristics Cp vs. λ for various values of the pitch angle β.*

Our wind turbine is coupled to a PMSG. Consequently, the electrical equations for the windings of the PMSG in a (*d*-*q*) frame are expressed by the following expressions:

$$\frac{d}{dt}\begin{pmatrix} i_{gd} \\ i_{gq} \end{pmatrix} = \begin{pmatrix} -\dfrac{R_s}{L_s} & \omega \\ -\omega & -\dfrac{R_s}{L_s} \end{pmatrix}\begin{pmatrix} i_{gd} \\ i_{gq} \end{pmatrix} + \begin{pmatrix} \dfrac{1}{L_s} & 0 \\ 0 & \dfrac{1}{L_s} \end{pmatrix}\begin{pmatrix} V_{gd} \\ V_{gq} \end{pmatrix} + \begin{pmatrix} 0 \\ -\dfrac{\omega\phi}{L_s} \end{pmatrix} \tag{7}$$

The expression of electromagnetic torque generated by this machine is given by:

$$C_{em} = p\phi i_{sq} \tag{8}$$

where R_s is the stator winding resistance, L_s is the stator winding inductance, i_{gd} and i_{gq} are the direct and quadratic stator currents, V_{gd} and V_{gq} are the direct and quadratic stator voltages, p is the number of pole pairs and ω (rd/s) is the electrical speed of the PMSG.

C. SC modeling

The SC is particularly an interesting storage means. It is characterized by a high specific power, a transfer of energy of short duration and a high yield [18]. The studied model is that of Zubieta and Bonert illustrated in Figureure 3a. This model is composed of a main RC branch at a fast storage that takes into account the energy aspect of the component during the charge and discharge phases, a second RC branch at a slow storage that considers the phenomenon of ionic redistribution during the resting phase, and an equivalent parallel R_2 resistance responsible for the phenomenon of self-discharge, also called "leakage resistance".

Some simplifying assumptions have been held in modeling without changing the electrical behavior of the component. The leakage resistance R_2 is eliminated due to its high value, and the effect of the slow branch is assumed negligible as well. Thus, the SC model is similar, as depicted in Figureure 3b, at a perfect capacitor C_1 and an equivalent series resistance R_1.

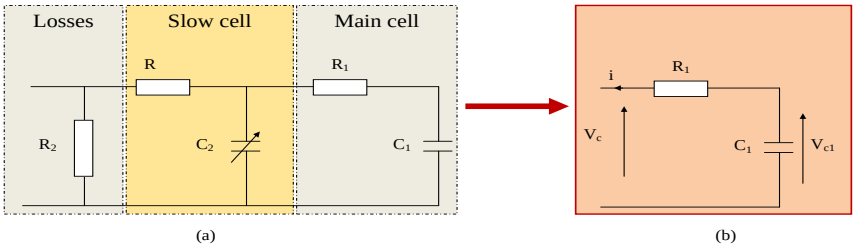

Figure. 3. *SC Model: (a) Model of Zubieta and Bonert, (b) Simplified model.*

The expression of the terminal voltage of a unitary SC is:

$$V_C = \frac{1}{C}\int i\,dt + i\,R_1 \tag{9}$$

The SC exploitation in high power applications requires connections in of multiple cells series and in parallel to reach the usable voltage level. Modeling a super-capacitor module comes first of all to model a unit cell. Thereafter, the arrangement one comes next to the other to create an SC bank. The total U_{sc} voltage across the SC is determined by the number of series formatting the N_s cells. Nevertheless, the resistance and the total capacity are determined thanks to the number of cells in series, N_s, and in parallel, N_p, as follows [19]:

$$\begin{cases} R_{sc} = R_1 \dfrac{N_s}{N_p} \\ C_{sc} = C_1 \dfrac{N_p}{N_s} \end{cases} \tag{10}$$

The SC module is connected to the DC bus through an inductive filter and a bidirectional current chopper. The objective of this filter lens is to create a current source at the chopper input and to smooth the SC charging and discharging current. The continuous modeling of this filter is given by the relationship below:

$$L_{sc}\frac{d}{dt}i_{sc} = U_{sc} - U_{m-sc} \tag{11}$$

where U_{m-sc} and L_{sc} are respectively the modulated voltage of the chopper and the equivalent inductance of the filter.

D. Modeling of load

In this study, decentralized generators are used to feed the load. The studied load is three-phased and of a balanced/linear type. It is modeled by a resistor R_L and an inductor L_L defined by the following expressions according to active and reactive powers, P_L and Q_L, required by the load:

$$\begin{cases} R_L = \dfrac{V_c^{\,2}.P_L}{P_L^{\,2} + Q_L^{\,2}} \\ X_L = L_L\omega_L = \dfrac{V_c^{\,2}.Q_L}{P_L^{\,2} + Q_L^{\,2}} \end{cases} \tag{12}$$

E. Modeling of RLC filter

The energy transfer from the DC bus to the load is ensured by a three-phase inverter. If the inverter is the only generator connected to an isolated load, an RLC filter should be interposed between the inverter and the receiver to obtain a quasi-sinusoidal voltage on its terminals. By neglecting the mutual inductances, the RLC filter represented in Figureure 1 is modeled according to the next equations:

$$\begin{cases} \frac{d}{dt} i_{fd} = -\frac{R_f}{L_f} i_{fd} + \omega_L i_{fq} + \frac{1}{L_f} V_{id} - \frac{1}{L_f} V_{cd} \\ \frac{d}{dt} i_{fq} = -\frac{R_f}{L_f} i_{fq} - \omega_L i_{fd} + \frac{1}{L_f} V_{iq} - \frac{1}{L_f} V_{cq} \\ \frac{d}{dt} V_{cd} = \frac{1}{C_f} i_{fd} + \omega_L V_{cq} - \frac{1}{C_f} i_{Ld} \\ \frac{d}{dt} V_{cq} = \frac{1}{C_f} i_{fq} - \omega_L V_{cq} - \frac{1}{C_f} i_{Lq} \end{cases} \quad (13)$$

where i_{Ld} and i_{Lq} are respectively the direct and quadratic components of the currents provided to the load.

$$\begin{cases} \frac{d}{dt} i_{Ld} = -\frac{R_L}{L_L} i_{Ld} + \omega_L i_{Lq} + \frac{1}{L_L} V_{cd} \\ \frac{d}{dt} i_{Lq} = -\frac{R_L}{L_L} i_{Lq} - \omega_L i_{Ld} + \frac{1}{L_L} V_{cq} \end{cases} \quad (14)$$

3. Power generation system control

The control of the studied production generator (wind turbine and SC) is achieved by controlling the power converters 1 and 2 and the DC bus. This strategy necessarily entails the control of the wind generator, the control of the SC, and the regulation of the DC bus voltage.

A. Robust nonlinear control of PMSG

The purpose of this paper is to present a comparative study between a classical vector control and a super-twisting second-order sliding mode control (SMC) for a PMSG.

In the first time, a classical vector control based on PI controllers is proposed. The purpose of this command is to show the sensitivity of the PI controllers against the high large range of wind speed variations. The structure of the classical vector control applied to our system is detailed in Figure 4.

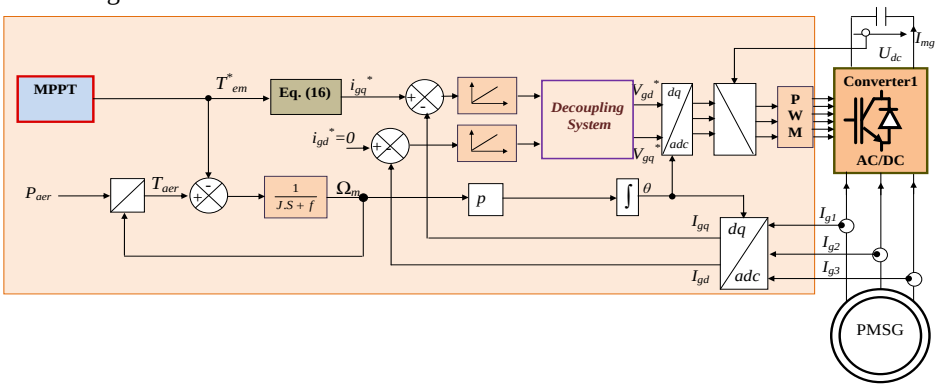

Figure 4. *Classical vector control of PMSG*

This PMSG control strategy, on the principle of imposing a reference of a direct current equal to zero, and on a reference of a quadratic current proportional to the reference's electromagnetic torque as follows:

$$\begin{cases} i_{gd}^{\ *} = 0 \\ i_{gq}^{\ *} = \dfrac{T_{em}^{\ *}}{p\phi} \end{cases} \tag{15}$$

In this work, the determination of T^*_{em} depends on the operation mode of the studied system. When the SC does not reach its maximum State Of Charge (SOC) "$U_{sc}<U_{scmax}$", the wind turbine operates in an MPPT to extract the maximum of power to supply load. Hence, the reference's electromagnetic torque is determined as:

$$T_{em}^{\ *} = T_{em-MPPT} = \frac{1}{2}\frac{\rho\pi R^5 C_{p-\max}}{\lambda_{opt}^{\ 3}}\Omega_m^{\ 2} \tag{16}$$

Once the module of the SC reaches its maximum SOC "$U_{sc}\geq U_{scmax}$", and the produced power exceeds the demanded power, the produced power becomes limited to provide only the demanded power by the load. Thereafter, the wind generator operates in Limited Power Point Tracking (LPPT). This limitation is due by the pitch angle β as follows:

$$\begin{cases} \beta_{ref} = 0 \; if \; U_{sc} < U_{sc\max}, P_g < P_n \\ \beta_{ref} = \dfrac{\Delta\beta}{\Delta P}\left(P_g - P_L\right) if \; U_{sc} > U_{sc\max}, P_g > P_L \\ \beta_{ref} = \dfrac{\Delta\beta}{\Delta P}\left(P_g - P_n\right) if \; P_g > P_n \end{cases} \tag{17}$$

with

$$\beta = \frac{1}{1+\tau_b.S}.\beta_{ref} \tag{18}$$

Due to the limited performance of the conventional vector control, in particular its sensitivity against strong wind speed variation, a SMC approach is proposed. This control is detailed in part 1 of Figure 5.

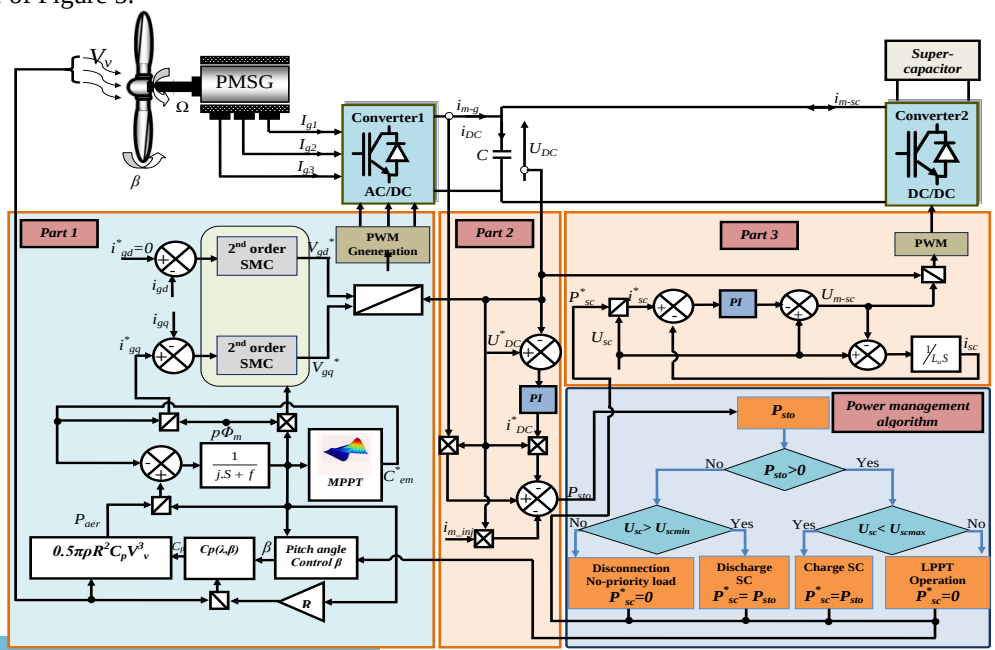

Figure 5. *Robust control of renewable power generation*

To illustrate the purposes of the SMC theory, a second-order nonlinear system with the following state equation is considered [20]:

$$\ddot{x} = f(x, \dot{x}) + g(x, \dot{x})u \tag{19}$$

where x and u are state and input vectors, and f and g are bounded nonlinear matrix functions of the system states.

In this section, we describe the different steps for implementing the control based on the super-twisting algorithm of a non-linear system. The objective of our study is to ensure the control and continuation of the trajectory of the reference y_r by the output y of the system, thus making the error $e=y_r-y$ tends towards zero in the presence of uncertainties and disturbances. For this, the sliding surface will be used to calculate the sliding variable can be rewritten as follows [21]:

$$\begin{aligned} S(x,t) &= \left(\frac{\partial}{\partial t} + \lambda\right)^{(n-1)} e \\ &= \sum_{k=0}^{n-1} \frac{(n-1)!}{k!(n-k-1)!} \left(\frac{\partial}{\partial t}\right)^{(n-k-1)} \lambda^k e \end{aligned} \tag{20}$$

where n is the system order and λ is a positive constant. The choice $\lambda>0$ guarantees a polynomial of Hurwitz.

The studied system in this paper is of a first order "$n=1$". Therefore, the sliding surface becomes:

$$S = e = y_r - y \tag{21}$$

The design of the control by the sliding mode takes into account the problems of stability and good performance in a systematic way in its approach.

The proposed control strategy also uses the super-twisting algorithm. The controller of a second-order SMC consists of three terms: The equivalent term $V_{sdq\text{-}eq}$ and the super-twisting terms U_{1dq} and U_{2dq}:

$$\begin{cases} V_{gd}^{*} = V_{gd-eq} + U_{1d} + U_{2d} \\ V_{gq}^{*} = V_{gq-eq} + U_{1q} + U_{2q} \end{cases} \tag{22}$$

To control the two components of the stator current, it is necessary to have two sliding mode controllers. In this context, we consider the sliding surfaces as follows:

$$\begin{cases} S_d = i_{gd}^{*} - i_{gd} \\ S_q = i_{gq}^{*} - i_{gq} \end{cases} \tag{23}$$

The equivalent term is obtained by the invariance conditions of the sliding surface:

$$\begin{cases} S_d = \dot{S}_d = -\frac{1}{L_s}\left(V_{gd} - R_s i_{gd} + \omega L_s i_{gq}\right) = 0 \\ S_q = \dot{S}_q = \frac{d}{dt} i_{gd}^{*} - \frac{1}{L_s}\left(V_{gq} - R_s i_{gq} - \omega L_s i_{gd} - \omega\phi\right) = 0 \end{cases} \tag{24}$$

Then, the equivalent term of each current control loop is:

$$\begin{cases} V_{gd-eq} = R_s i_{gd} - \omega L_s i_{gq} \\ V_{gq-eq} = \frac{d}{dt} i_{gd}^{*} + R_s i_{gq} + \omega L_s i_{gd} + \omega\phi \end{cases} \tag{25}$$

The two terms of the super-twisting control law are defined as follows [22]:

$$\begin{cases} U_{1d} = \int \alpha_d sign(S_d); U_{2d} = \beta_d |S_d|^{\frac{1}{2}} sign(S_d) \\ U_{1q} = \int \alpha_q sign(S_q); U_{2q} = \beta_q |S_q|^{\frac{1}{2}} sign(S_q) \end{cases} \quad (26)$$

The parameters α_d, α_q, β_d and β_q are determined by the second derivative of the sliding surface [23]:

$$\begin{cases} \ddot{S}_d = \varphi_d(x,t) + \gamma_d(x,t)\dot{V}_{dg} \\ \ddot{S}_q = \varphi_q(x,t) + \gamma_q(x,t)\dot{V}_{qg} \end{cases} \quad (27)$$

where *sign(S)* is a sign function defined as.

$$sign(S) = \begin{cases} 1 & if \quad S > \zeta \\ \dfrac{S}{\zeta} & if \quad S \geq |\zeta| \\ -1 & if \quad S < \zeta \end{cases} \quad (28)$$

Accordingly the convergence of S_d and S_q is guaranteed to zero in the presence of uncertainties and disturbances. The functions $\varphi_d(x,t)$, $\varphi_q(x,t)$, $\gamma_d(x,t)$ and $\gamma_d(x,t)$ must satisfy the following conditions: $\varphi_i>0$, $0<\Gamma_{mi}<\gamma_i<\Gamma_{Mi}$, $|\varphi_i|>\Phi_i$ where $i=d, q$.
where ζ is the width of the boundary layer.

The parameters α_d, α_q, β_d and β_q satisfy the next inequalities [24]:

$$\begin{cases} \alpha_i > \dfrac{\phi_i}{\Gamma_{mi}} \\ \beta^2{}_i \geq \dfrac{4\phi_i \Gamma_{Mi}(\alpha_i + \phi_i)}{\Gamma^3{}_{mi}(\alpha_i - \phi_i)} \end{cases}; i = d, q \quad (29)$$

To determine the required condition for the existence of the sliding mode, it is fundamental to design the Lyapunov function. Hence, the following Lyapunov function is defined as [14]:

$$\Upsilon = \frac{1}{2}S_d^2 + \frac{1}{2}S_q^2 \quad (30)$$

The system will be stable when the derivative of the Lyapunov function is negative:

$$\dot{\Upsilon} = S_d \dot{S}_d + S_q \dot{S}_q < 0 \quad (31)$$

On the other hand:

$$\begin{aligned} S_d \dot{S}_d &= -S_d \frac{1}{L_s}\left(R_s i_{gd} - \omega L_s i_{gq} + U_{1d} + U_{2d} - R_s i_{gd} + \omega L_s i_{gq}\right) \\ &= -S_d \frac{1}{L_s}\left(U_{1d} + U_{2d}\right) < 0 \end{aligned} \quad (32)$$

Likewise for the second sliding surface:

$$S_q \dot{S}_q = -S_q \frac{1}{L_s}\left(U_{1q} + U_{2q}\right) < 0 \quad (33)$$

Consequently, the global asymptotical stability is ensured and the speed control tracking is achieved.

$$\dot{\Upsilon} = -S_d \frac{1}{L_s}\left(U_{1d} + U_{2d}\right) - S_q \frac{1}{L_s}\left(U_{1q} + U_{2q}\right) < 0 \tag{34}$$

B. DC bus and SC power management

When the power provided by the wind turbine is higher than that required by the load "$P_g > P_L$" and the SC does not reach its maximum SOC "$U_{sc} < U_{scmax}$", it is the charging mode of the SC (Mode 1 is active). The reference power applied to the super-capacitors module is: "$P^*_{sc} = P_g - P_L$". In this condition the wind turbine operates in an MPPT.

When the power provided by the wind turbine is insufficient to meet the needs and the SC does not reach its minimum SOC "$U_{sc} > U_{scmin}$", it is a discharge mode of SC (Mode 2 is active). In this condition, the SC module will discharge to compensate this gap and ensure a balance between production and consumption. In this mode the reference power applied to the SC module is as follows: "$P^*_{sc} = P_g - P_L$". In this condition, the wind turbine operates in MPPT.

When the SC module reaches its maximum SOC "$U_{sc} \geq U_{scmax}$", and the produced power exceeds the demanded one. In this case, the wind generator operates in a LPPT to provide only the power demanded by the load (Mode 3 is active). This limitation is made by the augmentation of the pitch angle β.

The power generation system operate in mode 4 when there is an under production "$P_g < P_L$" and the ESS attends is minimum SOC "$U_{sc} \leq U_{scmin}$". In this mode, the no-priority load is disconnected in order to ensure the balance between production power and consumer one and limit the SOC of SC in U_{scmin}.

The role of the SC control presented in part 2 of Figureure 5 is to maintain the current charge or discharge I_{sc} current equivalent to its reference $I_{sc\text{-}ref}$ using a PI controller. This reference current is imposed by the power management algorithm above.

$$U_{m-sc} = U_{sc} - PI\left(I_{sc-ref} - I_{sc}\right) \tag{35}$$

In order to fix the direction of charging and discharging current and to adjust the level of the modulated voltage $U_{m\text{-}sc}$ to the DC bus voltage U_{bus}, the reversible DC/DC converter is controlled by the conversion function m_{sc} as follows:

$$m_{sc} = \frac{U_{m-sc}}{U_{bus}} \tag{36}$$

The power transits between the distribution generator and converter 3 must be provided through the DC bus. The DC bus is modeled by the following equations:

$$U_{bus} = \frac{1}{C_{bus}} \int i_{bus} dt = \frac{1}{C_{bus}} \int \left(I_{mg} - I_{mL} - I_{m-sc}\right) dt \tag{37}$$

where $I_{m\text{-}g}$ is the modulated current by the wind turbine, I_{mL} is the modulated current by the load, $I_{m\text{-}sc}$ is the modulated current by the SC, and I_{bus} and U_{bus} are respectively the current and voltage of the DC bus.

Part 2 of Figure 5 represents the DC bus controller block. A PI controller is applied to maintain the measured voltage U_{bus} equivalent to the reference U_{busref}. The U_{bus} voltage will be kept constant only if the DC bus power P_{bus} is zero. This condition will exist when the balance between the produced power and the required one is maintained in any condition.

Load side converter control

The inverter (converter 3 DC/AC) is coupled to the load through a filter formed by the combination of capacitance and inductance. Their aim is to prevent current harmonics caused by switching. To achieve a greater harmonic attenuation with the minimum cost, several filter topologies are developed such as the RL, the RLC and the LCL filters. In what follow, we are interested in the filter that is mostly used in the literature and which is a second-order RLC filter. Besides, PI controllers are used to adjust the output voltages of the inverter with the voltages at the RLC filter terminals and to control the current supplied by the inverter. Consequently, we are interested in the development of two control loops. The first one is for controlling the load

supply voltages and the second one is for monitoring the current injected by the inverter. Monitoring the load supply voltages provides a current that will serve as a reference for the current regulation loop provided by the inverter.

A. Voltage control loop

The block diagram of the voltage controller is illustrated in Figureure 6 "voltage control loop". The differential algebraic equations of the voltage controller are [25]:

$$\begin{cases} \phi_{cd} = V_{cd}^{*} - V_{cd} \\ \phi_{cq} = V_{cq}^{*} - V_{cq} \end{cases} \tag{38}$$

$$\begin{cases} i_{fd}^{*} = \left(k_p(v) + \dfrac{k_i(v)}{s} \right) \phi_{cd} - V_{cq} \omega_L C_f + F i_{Ld} \\ i_{fq}^{*} = \left(k_p(v) + \dfrac{k_i(v)}{s} \right) \phi_{cq} + V_{cd} \omega_L C_f + F i_{Lq} \end{cases} \tag{39}$$

where $k_p(v)$ and $k_i(v)$ are respectively the proportional and integral gains of the voltage controller, F is the feed-forward gain known also as the virtual impedance that can be calculated from the line and filter resistances, ω_L is the nominal frequency, and Φ_{cd} and Φ_{cq} are the errors at the input of voltages' controllers.

B. *Current control loop*

The block diagram of the current controller is represented in Figureure 6 "current control loop". The differential algebraic equations of the current controller are [25]:

$$\begin{cases} \psi_{fd} = i_{fd}^{*} - i_{fd} \\ \psi_{cq} = i_{fq}^{*} - i_{fq} \end{cases} \tag{40}$$

$$\begin{cases} V_{id}^{*} = \left(k_p(i) + \dfrac{k_i(i)}{s} \right) \psi_{fd} - i_{fq} L_f \omega_L \\ V_{iq}^{*} = \left(k_p(i) + \dfrac{k_i(i)}{s} \right) \psi_{fq} + i_{fd} L_f \omega_L \end{cases} \tag{41}$$

where $k_p(i)$ and $k_i(i)$ are respectively the proportional and integral gains of the current controllers, and ψ_{cd} and ψ_{cq} are the errors at the input of the current controllers.

C. Calculating of controller parameters

The loops for regulating the voltages at the terminals of the RLC filter capacitors are depicted in Figure 6. These regulators are identical because the transfer function is similar in the two axes, d and q.

The shape of the PI regulator used in this loop is as follows:

$$PI(v) = k_p(v) + \frac{k_i(v)}{s} = k_p(v) \left(\frac{1 + \tau_v s}{\tau_v s} \right); \tau_v = \frac{k_p(v)}{k_i(v)} \tag{42}$$

By calculating the closed-loop transfer function $G(v)$, we obtain:

$$G(v) = \frac{\dfrac{1}{C_f s} k_p(v) \left(\dfrac{1 + \tau_v s}{\tau_v s} \right)}{1 + \dfrac{1}{C_f s} k_p(v) \left(\dfrac{1 + \tau_v s}{\tau_v s} \right)} = \frac{1 + \tau_v s}{1 + \tau_v s + \dfrac{\tau_v C_f}{k_p(v)} s^2} \tag{43}$$

In order to determine the gain $k_p(v)$ and the time constant τ_v of the studied regulator, we identify the denominator of the function $G(v)$ with the second-order polynomial presented in expression (44). This polynomial has a minimum response time for ξ=0.7071, $t_r w_n$=3.

$$D = 1 + \frac{2\xi}{w_n} s + \frac{1}{w_n^2} s^2 \tag{44}$$

In this case, we obtain:

$$\begin{cases} k_p(v) = \dfrac{6\xi}{t_r} C_f \\ \tau_v = \dfrac{2\xi}{3} t_r \end{cases} \tag{45}$$

The parameters of the current regulators supplied by the inverter are determined in the same way as the voltage regulation loop.

The shape of the PI regulator used in this loop is as follows:

$$PI(i) = k_p(i) + \frac{k_i(i)}{s} = k_p(i)\left(\frac{1+\tau_i s}{\tau_i s}\right); \tau_i = \frac{k_p(i)}{k_i(i)} \tag{46}$$

By calculating the closed-loop transfer function *G(i)*, we get:

$$G(i) = \frac{\dfrac{1}{L_f s} k_p(i)\left(\dfrac{1+\tau_i s}{\tau_i s}\right)}{1 + \dfrac{1}{L_f s} k_p(i)\left(\dfrac{1+\tau_i s}{\tau_i s}\right)} = \frac{1+\tau_i s}{1+\tau_i s + \dfrac{\tau_i L_f}{k_p(i)} s^2} \tag{47}$$

Finally, we obtain:

$$\begin{cases} k_p(i) = \dfrac{6\xi}{t_r} L_f \\ \tau_i = \dfrac{2\xi}{3} t_r \end{cases} \tag{48}$$

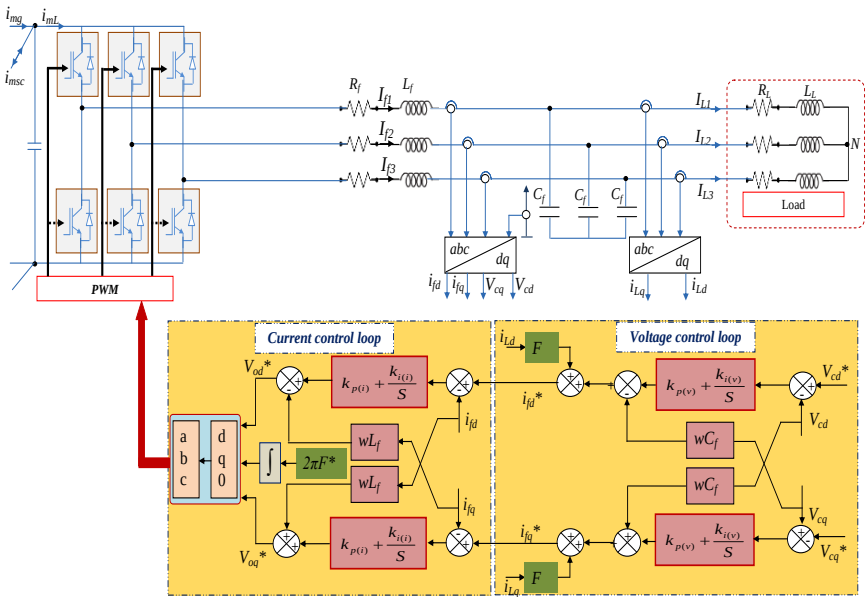

Figure 6. *Load side converter control*

5. Simulation results

In this section, the simulation and analysis of the studied system as well as the proposed control strategy will be presented and commented through Matlab/Simulink software.

The evolution of our control strategy is implemented under the following conditions:

- Wind speed profile realistic provided in Figure 7a.
- Active demanded power shown in Figure 7c.
- Reactive demanded power shown in Figure 7d.

In this simulation, the interaction between the different sources of a decentralized generator to manage the various paths of the power flow and the power exchange between our generator and the charge will be proven.

A wind turbine is designed to rotate at a nominal speed and produce a nominal power. For this, a control system called 'pitch angle' is inserted in order to control the power output of the wind turbine and thus limiting it when the wind speed is high. The operation of this control system is summarized as follows: When the wind speed exceeds its nominal value, this β angle (Figureure 7b) will increase, hence getting a decrease of a power coefficient C_p. Therefore, a limitation of the produced power is achieved (Figureure 8a). In addition, when the SC module reaches its maximum SOC "$U_{sc} \geq U_{scmax}$" and the produced power exceeds the demanded power, the wind generator will operate in an LPPT to provide only the power demanded by the load. This limitation is made by the augmentation of the pitch angle β.

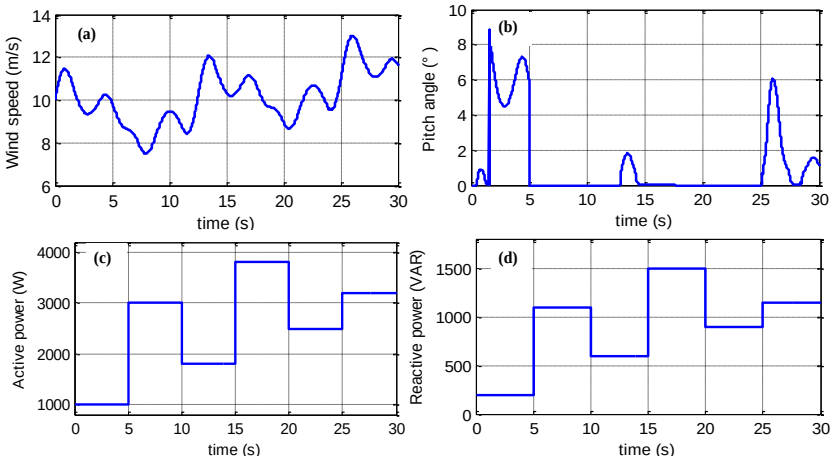

Figure 7. (a) Wind speed, (b) Pitch angle β, (c) Demanded active power, (d) Demanded reactive power

Figure 8a demonstrates the variation of active powers during the various system operating modes. The blue allure indicates the power generated by the PMSG. This power should be maximized by the MPPT algorithm and it will become equal to the demanded power when there is an excess of production and the storage system reaches its maximum SOC. The red allure corresponds to the power required by the load. The brown allure presents the charge and discharge power of the SC. We clearly remark after these Figureures that the balance between the generated and consumed powers is reached. Subsequently, one obtains a constant DC bus voltage at 400V, as pointed out in Figureure 9b.

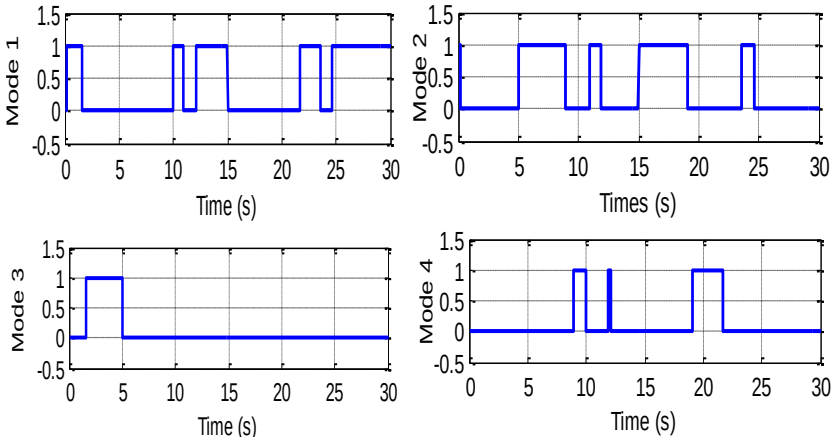

Figure 8. Different interactive cases of the deduced modes

During the periods [0.2, 158], [10, 10.9], [12, 15], [21.7, 23.6] and [24.6, 30] the SC charge mode is activated (mode 1). In this mode there is an excess of production "$P_g > P_L$". This excess is absorbed by the SC since it does not reach its maximum SOC "$U_{sc} < U_{scmax}$". During the periods [0, 0.2], [5, 8.9], [10.9, 11.9], [15, 19.1] and [23.6, 24.6] the SC discharge mode is activated (mode 2). In this mode there is a lack of production "$P_g < P_L$". This lack is compensated by the SC since it does not reach its minimum SOC "$U_{sc} > U_{scmin}$". During the interval [1.58, 5] mode 3 is active. In this mode the storage system reaches its maximum SOC "$U_{sc} \geq U_{scmax}$" and the wind turbine generates an excess power. Here, the LPPT mode correlates the production to consumption and fixes the SOC of the storage system to its maximum limit. In the time intervals [8.9, 10], [11.9, 12] and [19.1, 21.7] mode 4 is active. In this mode the power generated by the PMSG is less than the needs, and the SC reaches its minimum state of charge "$U_{sc} \leq U_{scmin}$". In this condition, the wind turbine ensures a continuous supply of priority loads. Finally, the SOC of the SC is presented in Figureure 8d. Figureure 8c indicates the performance of the used PI controller to control the charge and discharge current of the SC.

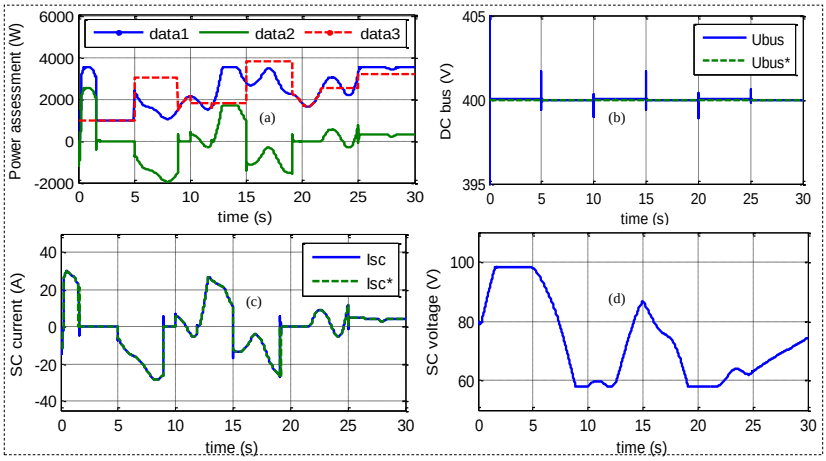

Figure 9. (a) Simulated power assessment, (b) DC-bus voltage, (c) SC current, (d) SC voltage

Finally, the inverter adjusts, using the PI correctors, the voltages (V_{cd}, V_{cq}) and currents (i_{fd}, i_{fq}) measured at the output of the RLC filter with the nominal condition (V_n , F_n). This adjustment is validated by the following Figures:

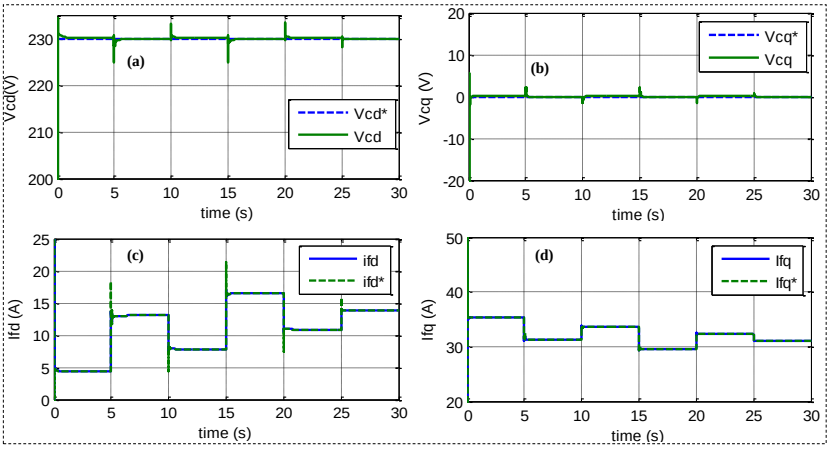

Figure 10. VSI simulation results, (a) V_{cd} voltage, (b) V_{cq} voltage, (c) i_{fd} current, (d) i_{fq} current.

The conventional PI control laws give good results in the case of linear systems. For nonlinear systems, these laws may be inadequate because they are not robust, especially when the demands on the accuracy and other dynamic characteristics of the system are severe. We must use control laws insensitive to an external disturbances and nonlinearities. The SMC, which is by its nature a nonlinear control, has this robustness. However, the performance of SMC is limited by the presence of the phenomenon of chattering caused by the use of a first order sliding mode. To work around this obstacle, a control by a higher-order sliding mode based on the super-twisting algorithm is proposed.

To evaluate the performance of these control techniques, a comparative study between a classical vector control and second-order SMC, based on the super-twisting algorithm, is presented. The results will be compared under the same operating conditions and for the same conFigureuration.

Figure 11a provides a comparison of the quadratic component of the stator current between the second-order SMC method and a conventional vector control. This test demonstrates that the second-order SMC is better than the PI control from a standpoint of response time and rejection disturbances. According to the electromagnetic torque produced by the machine, depicted by Figure 11b, the suggested regulator has several advantages than the PI control, such as fast dynamic response and robustness at uncertainties, at external disturbances, and at high range of wind speed variation.

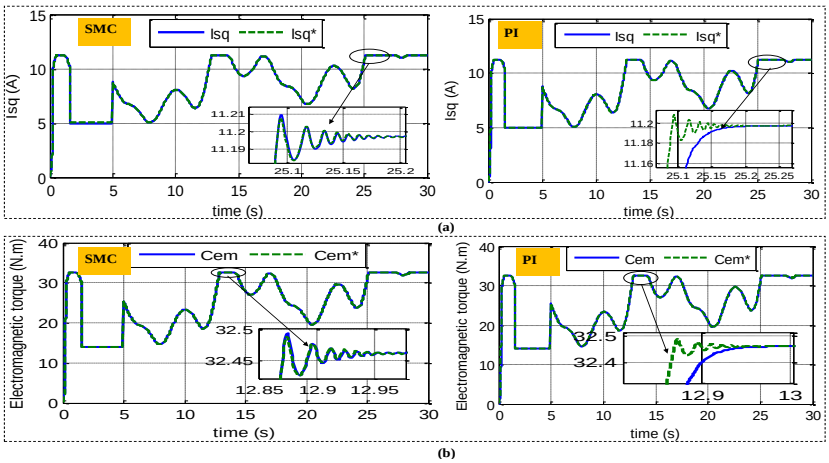

Figure 11. (a) Quadrature component of stator current i_{sq}, (b) Electromagnetic Torque C_{em}

Note that the system operates in sliding practically exhibits no chattering and proves the robustness of the controller in the presence of the aforementioned disturbances. Illustratively, the trajectory of the controlled system in the state space ($S - \dot{S}$ plane) is presented in Figure 12.

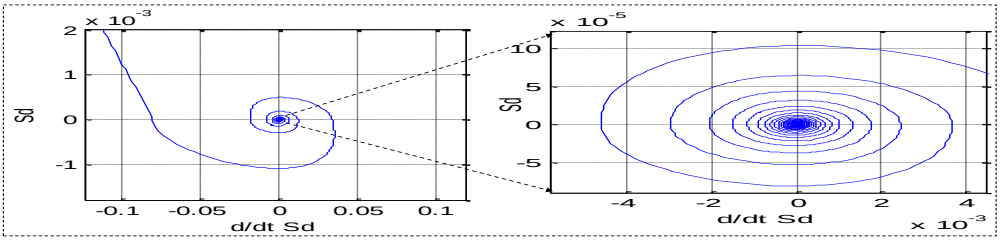

Figure 12. $S - \dot{S}$ plane

6. Conclusions

In this paper, we have validated the ability of a renewable wind generator to power load in the presence of variations in production. The validation has been proven by combining an SC module able to act in real time depending on the variations of generated and consumed powers. Three power converters have been used. In fact, a control strategy based on the command of this three power converters has been developed. A second-order SMC based on the super-twisting algorithm has been applied to the PMSG which would keep developing control signals applied to converter 1, which would enable the extraction of the maximum power of the wind turbine. It has aimed to guarantee a robust control strategy that would give a good performance despite the wide range of the external disturbance and the uncertainties of the different components of the wind system. The control of converter 2 is responsible for regulating the DC bus voltage by generating or storing energy with the SC module to compensate for the intermittent nature of the wind power and to ensure a continuous supply of load. The DC bus power is transferred to the load through converter 3. The interest of converter 3 is to adjust the capacitors voltages and the output currents of the RLC filter with the nominal frequency and voltage. The results obtained by simulation show the performance of this control strategy to attend a wind generator in order to ensure a continuous supply of loads despite the form intermittence of its main source.

7. References

[1]. R. Kallel, G. Boukettaya, L. Krichen, “Demand side management of household appliances in stand-alone hybrid photovoltaic system”, Renewable Energy, 2015, vol. 81, pp. 123-135.

[2]. M. Z. Jacobson, M. A. Delucchi. : “Providing all global energy with wind, water, and solar power, Part I: Technologies, energy resources, quantities and areas of infrastructure, and materials”, Energy Policy, 2011, vol. 39, pp. 1154–1169.

A. Masmoudi, A. Abdelkafi, L. Krichen. “Electric power generation based on variable speed wind turbine under load disturbance”, Energy, 2011, vol. 36, pp. 5016-5026.

[3]. N. Mendis, KM. Muttaqi, S. Perera. “Active power management of a super-capacitor-battery hybrid energy storage system for standalone operation of DFIGURE based wind turbines”. IEEE, industry applications society annual meeting (IAS), 2012. pp. 1-8.

[4]. Z. Cabrane, M. Ouassaid, M. Maaroufi, “Analysis and evaluation of battery-supercapacitor hybrid energy storage system for photovoltaic Installation”, International Journal of Hydrogen Energy - Elsevier, 2016, pp. 1-11.

[5]. S. Hmam, J.C. Olivier, S. Bourguet, L. Loron, “A cycle-based and multirate approach for power system simulation application to the ageing estimation of a supercapacitor-based ferry”, Journal of Energy Storage, 2016, vol. 8, pp. 175–184.

[6]. S. K. Ayyappa, D. N. Gaonkar, "Performance Analysis of a Variable-speed Wind and Fuel Cell-based Hybrid Distributed Generation System in Grid-connected Mode of Operation", Electric Power Components and Systems, 2016, pp.1-10.
[7]. N. A. Ahmed, M. Cameron, "The challenges and possible solutions of horizontal axis wind turbines as a clean energy solution for the future," Journal of renewable and sustainable Energy, 2014, vol. 38, pp. 439-460.
[8]. N. Bhende, S. Mishra, S. G. Malla, "Permanent Magnet Synchronous Generator-Based Standalone Wind Energy Supply System," IEEE Transactions on Sustainable Energy, 2011, vol. 38, pp. 439-460.
[9]. M. Mansour, M. N. Mansouri, M. F. Mmimouni, "Study and Control of a Variable-Speed Wind-Energy System Connected to the Grid" international journal of renewable energy research, 2011, vol. 1, no. 2, pp. 96-104.
[10]. A. Rezvani, M. Izadbakhsh, M. Gandomkar, "Enhancement of hybrid dynamic performance using ANFIS for fast varying solar radiation and fuzzy logic controller in high speeds wind", Journal of electrical systems, 2015, vol. 11, n°. 1, pp. 11-26.
[11]. S. M. Muyeen, Ahmed Al – Durra: "Modeling and control strategies of fuzzy logic controlled inverter system for grid interconnected variable speed wind generator," IEEE Syst. J, 2013, vol.7, n°. 4, pp. 817-824.
[12]. M. Dansoko, H. Nkwawo, B. Diourté, F. Floret, R. Goma, G. Kenné.: "Robust multivariable sliding mode control design for generator excitation of marine turbine in multi-machine conFigureuration," Electrical Power and Energy Systems, 2014, vol. 63, pp. 423–428.
[13]. Y. Errami, M. Ouassaid, M. Maaroufi.: 'A performance comparison of a nonlinear and a linear control for grid connected PMSG wind energy conversion system', Electrical Power and Energy Systems, 2015, vol. 68, pp. 180–194.
[14]. M. A. Abdullah, A. H. M. Yatim, T. C. Wei. "A study of maximum power point tracking algorithms for wind energy system". IEEE first conference on Proceedings of clean energy and technology (CET), 2011, p. 321–326.
[15]. Y. WANG, "Evaluation de la Performance des Réglages de Fréquence des Eoliennes à l'Echelle du Système Electrique : Application à un Cas Insulaire ", thèse de doctorat préparée au L2EP Ecole Centrale de Lille, soutenue à Lille, France, 20 novembre 2012.
[16]. M. Smaoui, L. Krichen, "Control, energy management and performance evaluation of desalination unit based renewable energies using a graphical user Interface," Energy, 2016, vol. 114, pp. 1187-1206.
[17]. Al. Mundy, L. P. Gregory, "Reduced-order physics-based modeling and experimental parameter identification for non-Faradaic electrical double-layer capacitors", Journal of Energy Storage, 2016, vol. 7 pp. 167–180.
[18]. R. Kallel, G. Boukettaya, L. Krichen, "Control Management Strategy of Stand-Alone Hybrid Power Micro-System using Super-Capacitor", International Journal of Renewable Energy Research, 2014, Vol. 4, n° 1, pp. 210-223.
[19]. S. M. Mozayan, M. Saad, H. Vahedi, H. Fortin-Blanchette, M. Soltani. "Sliding Mode Control of PMSG Wind Turbine Based on Enhanced Exponential Reaching Law", IEEE Transactions on Industrial Electronics, 2016, vol. 63, n°. 10, pp. 6148-6159.
[20]. M. Derbeli, M. Farhat, O. Barambones, L. Sbita.: 'Control of PEM fuel cell power system using sliding mode and super-twisting algorithms'. International journal of hydrogen energy, 2016, pp.1-12.
[21]. Evangelista, V. Fernando, P. Paul.: "Active and reactive power control for wind turbine based on a MIMO 2-sliding mode algorithm with variable gains". IEEE Transactions on Energy Conversion, 2013, vol. 28, n°. 3, pp. 682–689.
[22]. S. Benelghali, M. El H. Benbouzid, J. F. Charpentier, T. Ahmed-Ali, I. Munteanu, "Experimental Validation of a Marine Current Turbine Simulator: Application to a Permanent Magnet Synchronous Generator-Based System Second-Order Sliding Mode Control", IEEE Transactions on Industrial Electronics, 2011, vol. 58, n° 1, pp. 118-126.

[23]. M. Benbouzid, B. Beltran, Y. Amirat, G. Yao, J. Han, H. Mangel. “Second-order sliding mode control for DFIGURE-based wind turbines fault ride-through capability enhancement”, ISA Transactions, 2014, vol. 53, pp. 827–833.
[24]. A. Bidram, A. Davoudi, F. L. Lewis, and J. M. Guerrero, “Distributed cooperative secondary control of microgrids using feedback linearization,” IEEE Transactions on Power Systems, 2013, vol. 28, pp. 3462–3470.